frontiers | Frontiers in Energy Research

BRIEF RESEARCH REPORT
published: 26 April 2022
doi: 10.3389/fenrg.2022.870329

Supported SnS_2 Nanosheet Arrays on Ni Foam for Supercapacitors

*Haibin Sun *†, Shuangshuang Liang†, Wenrui Zheng, Congcong Liu, Chao Zhang, Zhichao Ji, Shenghong Liu and Wenhe Xie*

Key Laboratory of Microelectronics and Energy of Henan Province, College of Physics and Electronic Engineering, Xinyang Normal University, Xinyang, China

Layered metal sulfides are regarded as potential candidates for supercapacitive electrode materials due to the unique spatial dimensions for charge transport. Herein, self-supported SnS_2 nanosheet arrays on nickel (Ni) foam were successfully fabricated *via* a facile solvothermal approach. Interestingly, the continuous and high-density SnS_2 nanosheet arrays are interconnected to form porous Ni@SnS_2 electrode materials, which suppress the self-aggregation of SnS_2 and provide outstanding conductivity with 3D-networked Ni framework. The Ni@SnS_2 electrode demonstrates a high areal specific capacitance of 1965.56 mF cm^{-2} at a current density of 1 mA cm^{-2} and satisfactory cycling stability (78.3% capacity retention after 10,000 cycles). This self-supported porous structure provides a promising way to build advanced electrode material for supercapacitors.

Keywords: SnS2 nanosheet arrays, crystal growth, self-supported, pseudocapacitors, energy storage and conversion

OPEN ACCESS

Edited by:
Vivekanand Shukla, Chalmers University of Technology, Sweden

Reviewed by:
Muhammad Sufyan Javed, Jinan University, China
Hai-Chao Chen, Qingdao University, China

****Correspondence:***
Haibin Sun
sunhaibin@xynu.edu.cn

†These authors have contributed equally to this work

Specialty section:
This article was submitted to Electrochemical Energy Conversion and Storage, a section of the journal Frontiers in Energy Research

Received: *06 February 2022*
Accepted: *21 March 2022*
Published: *26 April 2022*

Citation:
Sun H, Liang S, Zheng W, Liu C, Zhang C, Ji Z, Liu S and Xie W (2022) Supported SnS_2 Nanosheet Arrays on Ni Foam for Supercapacitors. Front. Energy Res. 10:870329. doi: 10.3389/fenrg.2022.870329

INTRODUCTION

Supercapacitors, due to their fast recharge rate, high power densities, and outstanding durability, have attracted considerable attention from scientists to industrialists (Javed et al., 2019; Zhang et al., 2019; Javed et al., 2020a; Fu et al., 2021). The energy storage mechanisms of supercapacitors can be divided into pseudocapacitors and electric double-layer capacitors. Among them, pseudocapacitors have attracted extensive interest because their Faradaic redox reaction can achieve a higher energy density than electric double-layer capacitors. In the past few years, transition metal oxides/hydroxides/sulfides including V_2O_5 (Javed et al., 2020b), MnO_2 (Bai et al., 2018), $Co.(OH)_2$ (Wang et al., 2016), and Ni_3S_2 (Xie et al., 2021), were mainly studied as pseudocapacitor electrode materials.

SnS_2, has been used as a promising electrode material for batteries, photocatalysts and supercapacitors. For example, Cao et al. designed and synthesized a N,S-doped carbon/SnS_2 nanosheets hybrid as an anode material for potassium ion batteries (Cao et al., 2021), Sun et al. prepared a graphene/SnS_2 hybrid material to enhance absorption in the visible region (Sun et al., 2019), and, Parveen et al. reported flower-like SnS_2 with a high specific capacitance (~ 431.82 F g^{-1} at 1 A g^{-1}) (Parveen et al., 2018). However, the agglomeration of 2D SnS_2 nanosheets seriously hinders the active sites and redox reaction as a supercapacitive electrode material over extended cycle.

Herein, we prepared self-supported SnS_2 nanosheet arrays on nickel foam (Ni@SnS_2) by a simple solvothermal method. In this architecture, the porous SnS_2 nanosheet arrays provided the fast charge transfer passages, and the 3D-networked Ni foam improved the high conductivity of the material, endowing the outstanding electrochemical performance overall. The as-prepared Ni@SnS_2 electrode exhibited a high capacity of 1965.56 mF cm^{-2} at 1 mA cm^{-2} and a long cycling life (78.3% retention after 10,000 cycles at 20 mA cm^{-2}).

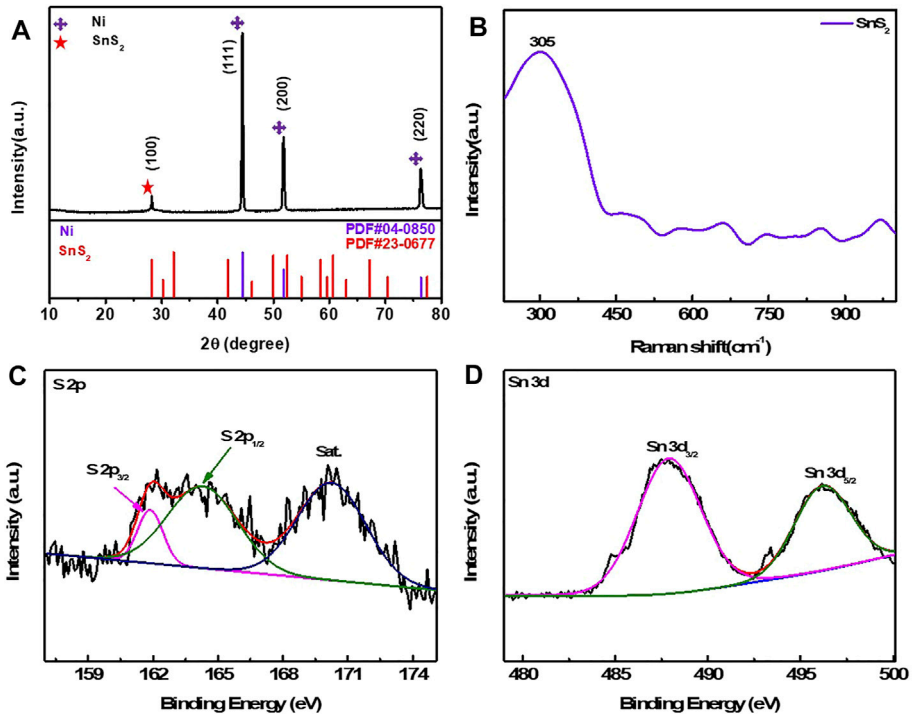

FIGURE 1 | (A) XRD pattern of the Ni@SnS_2 nanosheet arrays; **(B)** Raman spectrum; XPS survey spectra of **(C)** S 2p and **(D)** Sn 3d.

EXPERIMENTAL

Synthesis of the Ni@SnS_2 Nanosheet Arrays

The nickel (Ni) foam was cleaned with acetone, anhydrous ethanol, and deionized water. First, 0.701 g of $SnCl_4.5H_2O$ and 0.225 g of thioacetamide (TAA) were added to 60 ml of glycol and stirred for 20 min to form a uniform solution. Then, the prepared solution and a piece of cleaned Ni foam were transferred to a 100 ml lined Teflon stainless steel autoclave and maintained at 130°C for 8 h. Afterward, the sample was taken out, cleaned with anhydrous ethanol and deionized water, and then placed in the oven at 60°C for 12 h to obtain Ni@SnS_2 samples.

Characterization

The morphology was characterized by cold field emission scanning electron microscopy (SEM, Hitachi 4,800) and transmission electron microscopy (TEM, JEM 2100F). The phase structure of the sample was analyzed by X-ray Powder Diffractometer (XRD, Rigaku D/Max-2400 diffractometer) and micro-Raman spectroscopy (Jobin-Yvon LabRAM HR800 UV, YAG 532 nm). The surface composition and chemical state of the sample are analyzed by X-ray photoelectron spectroscopy (XPS, K-ALPHA 0.5 eV). The specific surface area was calculated by the Brunauer-Emmett-Teller (BET) method. The pore size distribution (PSD) was derived from the adsorption branches of isotherms by the Barrett-Joyner-Halenda (BJH) method.

Electrochemical Measurements

The electrochemical performance was measured using an electrochemical workstation (CHI660e). Ni@SnS_2 was directly used to test the electrochemical performance of three electrodes. Saturated calomel was used as the reference electrode, a platinum electrode was used as the counter electrode, Ni@SnS_2 (1×1 cm^2) was used as the working electrode, and 2 M KOH was used as the electrolyte. Ni@SnS_2 was tested by cyclic voltammetry (CV, sweep speed 5–100 mV s^{-1}) and constant current charge-discharge curves (GCD, current density 1–100 mA cm^{-2}). Electrochemical impedance spectroscopy (EIS) was performed at AC frequency of 0.01 Hz–100 kHz and an amplitude of 5 mV.

RESULTS AND DISCUSSION

Composition and Morphology Analysis

Figure 1Ashows the XRD patterns of the Ni@SnS_2 nanosheet arrays. As is seen, the strong diffraction peaks centered at 44.5°, 51.7°, and 76.3°, correspond to the (111), (200), and (220) crystalline facets of Ni foam (PDF#04-0850), respectively. Due to the weak peak intensity, the characteristic reflection at 28.1° can be assigned to the (100) plane of SnS_2 (PDF#23-0677) (Li et al., 2018). In compared to the SnS_2 samples left from the Ni foam (**Supplementary Figure S1**), the pure SnS_2 samples (**Supplementary Figure S2**) exhibit the same diffraction peaks in the XRD patterns, confirming the existence of SnS_2 used as real active materials. Raman spectrum (**Figure 1B**) proves the

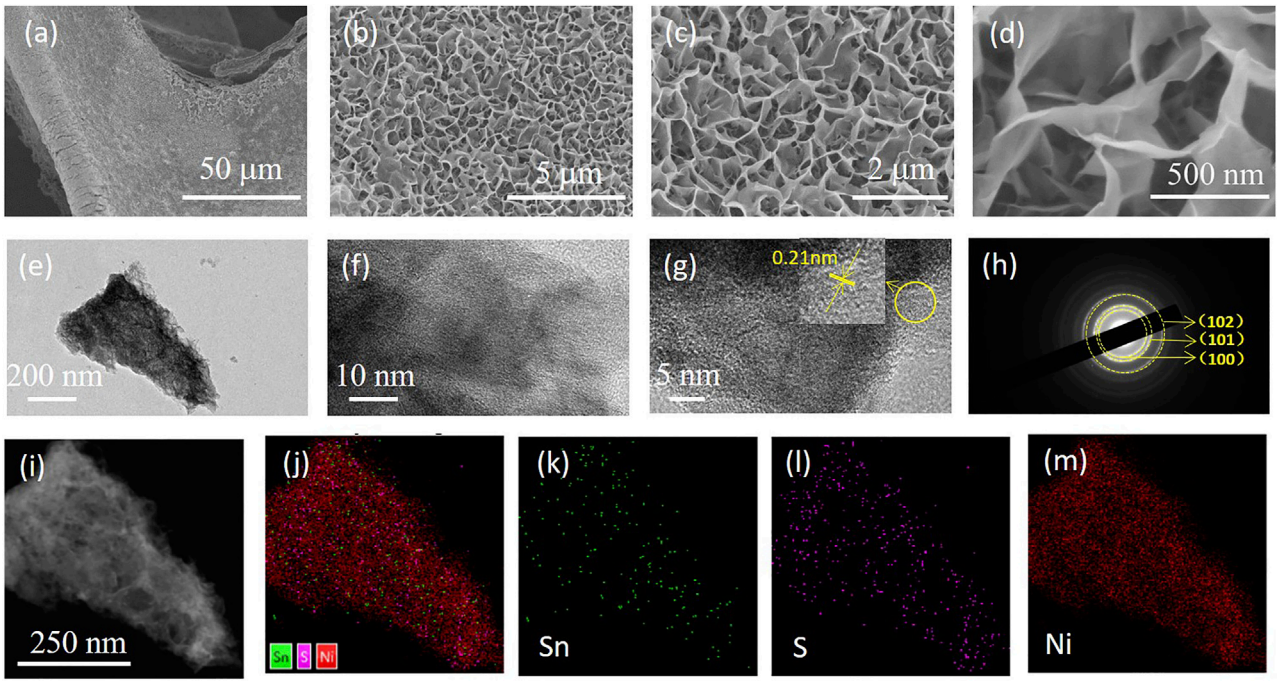

FIGURE 2 | (A–D) SEM images at different magnifications of the Ni@SnS_2 nanosheet arrays; **(E–G)** TEM images at different magnifications; **(H)** SAED pattern; **(I–M)** Elemental mappings.

existence of SnS_2 on the surface of Ni foam with a high band at ~ 305 cm^{-1}, which is assigned to the A_{1g} mode of SnS_2 (Jiang et al., 2013; Qu et al., 2014). Furthermore, **Supplementary Figure S3** shows the XPS full survey spectrum, confirming the existence of Sn, Ni, and S elements. In the high-resolution narrow spectrum of S 2p (**Figure 1C**), the two peaks located at 161.9 and 163.1 eV respectively correspond to S $2p_{3/2}$ and S $2p_{1/2}$, accompanying the satellite peak. The Sn 3d spectrum (**Figure 1D**) contains two-orbit peaks at 487.1 and 495.4 eV, corresponding to Sn $3d_{3/2}$ and Sn $2d_{5/2}$. The BET surface area and pore size distribution of Ni@SnS_2 were conducted by nitrogen isothermal adsorption/desorption measurement. The typical type IV isotherm curves (**Supplementary Figure S4A**) exhibit the evident hysteresis loop and the according surface area is about 1.14 $m^2 \cdot g^{-1}$. The pore diameter (**Supplementary Figure S4B**) is located at 2.17 and 10.97 nm, indicating the existence of mesoporous structure.

Figures 2A–D display the morphological features of the Ni@SnS_2 nanosheet arrays by SEM. In the low-magnification SEM image (**Figure 2A**), a homogeneous and complete SnS_2 nanosheet arrays coated the skeleton of the Ni foam. **Figures 2B–D** show the high-magnification SEM images, revealing that the vertically aligned SnS_2 nanosheets are highly packed on the Ni foam and are interconnected to form numerous porous structures. A single Ni@SnS_2 nanosheet array was further observed by TEM. **Figures 2E,I** show images of the intersected SnS_2 nanosheet structures, which are consistent with the SEM analysis. From the high-resolution TEM (HRTEM) image, **Figures 2F,G** shows a lattice fringe of 0.21 nm, corresponding to the (102) plane of SnS_2. The selected area electron diffraction (SAED) pattern is shown in **Figure 2H**, implying that the polycrystalline rings can be indexed to the (101), (100) and (102) planes of SnS_2 (Liu et al., 2021). Furthermore, elemental mappings (**Figures 2I–M**) were measured to demonstrate the porous structure and homogeneous distribution of Sn, and S supported on Ni foam.

Electrochemical Properties

Figure 3A shows a typical Ni@SnS_2 electrode with a pair of redox peaks at a scan rate of 5 mV s^{-1}. With increasing scan rates, the shapes of these CV curves nearly retain their initial state when the scan rate is as high as 100 mV $s-^{1}$. As shown in **Figure 3B**, the GCD curves of the samples display almost symmetric shapes at all current densities from 1 to 100 mA $cm-^{2}$, suggesting ideal pseudocapacitance properties (Li et al., 2021).

When current density was increased from 1 to 100 mA $cm-^{2}$ (**Figure 3C**), the specific capacitance decreased from 1965.56 to 733.78 mF $cm-^{2}$. Furthermore, 75% of the initial specific capacitance was maintained even at a high current density of 20 mA $cm-^{2}$. Here, the specific capacitances of bare Ni foam measured in **Supplementary Figure S5** show much less than to the values of Ni@SnS_2 electrode, suggesting the ignorable influence. The following relationship (Bian et al., 2022) is established between the peak current i) and scan rate (v): $i = av^b$, where a and b are constants. As shown in **Supplementary Figure S6**, the b-values of the anodic and cathodic peaks are 0.548 and 0.531, respectively, reflecting the diffusion-controlled

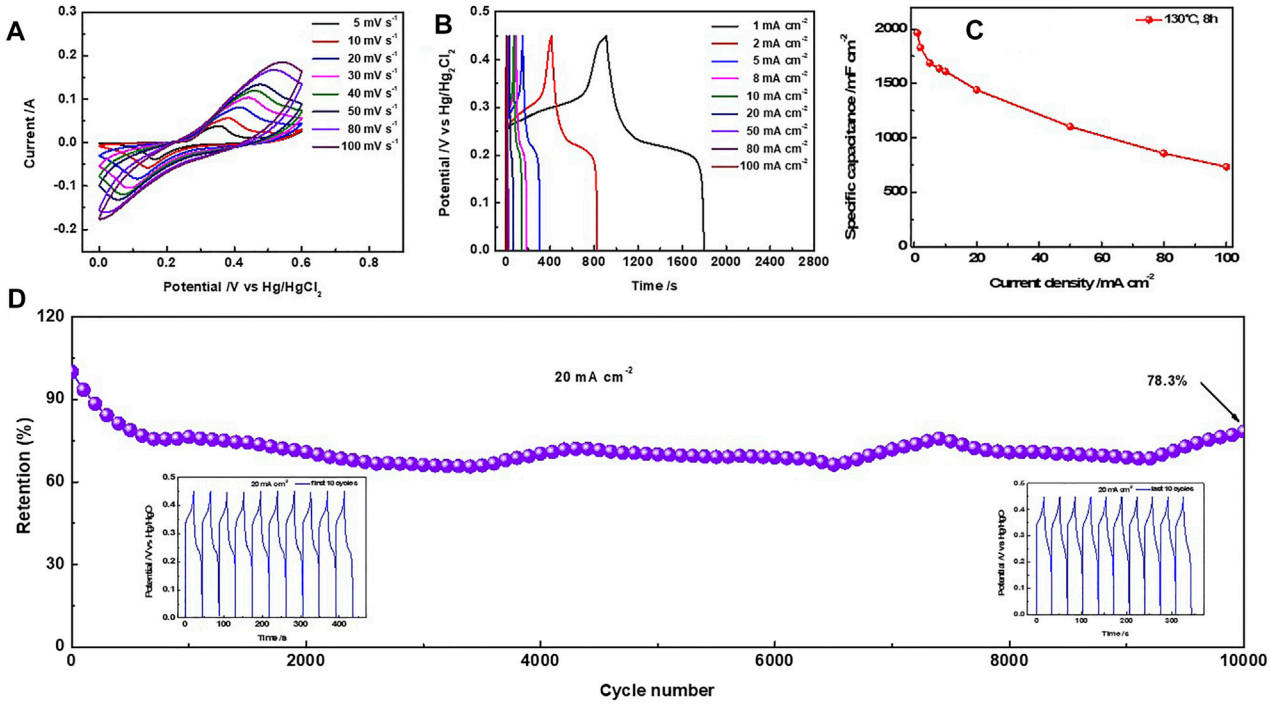

FIGURE 3 | (A) CV curves of the Ni@SnS_2 nanosheet arrays at different scan rates; **(B)** GCD curves; **(C)** Rate performance; **(D)** Cycle stability at 20 mA cm^{-2} (inset: the lower left corner shows the GCD curves of the first 10 cycles, and the lower right corner shows the GCD curves of the last 10 cycles).

behavior in the charge storage process. The cycle stability of the Ni@SnS_2 electrode shown in **Figure 3D** was measured by the GCD method at a high current density of 20 mA cm^{-2}. After 10,000 cycles, the capacitance retains 78.3% of its initial value, displaying its excellent application potential. Compared with the SEM images of the Ni@SnS_2 electrode after the long cycle (**Supplementary Figure S7**), the nanosheet arrays were partly retained while the morphologies of Ni foam were dilapidated, decreasing the active site of the electrode material and causing the capacity decay after 10,000 cycling tests. According to the EIS Nyquist plots of the Ni@SnS_2 electrode (**Supplementary Figure S8**), the real axis intercepts in the high-frequency region show a solution resistance (Rs) of about 1.0 Ω. The quasi-semicircle arc in the high-to-medium-frequency region corresponds to the charge transfer resistance (R_{ct}). Notably, the samples possessed a higher R_{ct} (3.968 Ω) compared with the initial R_{ct} (0.85 Ω) after a long cycle, indicating the increased electrochemical system resistance of the electrode material.

CONCLUSION

Porous Ni@SnS_2 nanosheet arrays were successfully prepared by a facile solvothermal method using Ni foam as the 3D framework. Due to the unique structure and crystal composition, the Ni@SnS_2 electrode exhibited remarkable supercapacitive performance with high specific capacity and good cycling stability.

DATA AVAILABILITY STATEMENT

The original contributions presented in the study are included in the article/**Supplementary Material**, further inquiries can be directed to the corresponding author.

AUTHOR CONTRIBUTIONS

HS: Conceptualization, Supervision SL: Data curation, Writing—original draft WZ and CL: Data analysis CZ and ZJ: Visualization, Investigation SL: Methodology WX: review and editing.

FUNDING

This work was supported by the National Natural Science Foundation of China (11874317), Key Scientific Research Projects of Colleges and Universities in Henan Province (22A140009), XYNU Excellent MD Students Major Foundation (2021KYJJ07) and Nanhu Scholars Program for Young Scholar of XYNU. This work made use of instruments in analysis testing center of XYNU.

SUPPLEMENTARY MATERIAL

The Supplementary Material for this article can be found online at: https://www.frontiersin.org/articles/10.3389/fenrg.2022.870329/full#supplementary-material

REFERENCES

Bai, X., Tong, X., Gao, Y., Zhu, W., Fu, C., Ma, J., et al. (2018). Hierarchical Multidimensional MnO_2 via Hydrothermal Synthesis for High Performance Supercapacitors. *Electrochimica Acta* 281, 525–533. doi:10.1016/j.electacta.2018.06.003

Bian, Z., Zhang, Z., Zhao, K., Li, K., Xiao, Q., Li, K., et al. (2022). 3D Net Carbon-Based Cobalt Sulfides for High-Performance Supercapacitors by a Simple, green and Convenient Method. *Mater. Lett.* 311, 131539. doi:10.1016/j.matlet.2021.131539

Cao, K., Wang, S., Jia, Y., Xu, D., Liu, H., Huang, K.-J., et al. (2021). Promoting K Ion Storage Property of SnS_2 Anode by Structure Engineering. *Chem. Eng. J.* 406, 126902. doi:10.1016/j.cej.2020.126902

Fu, J., Jiang, X., Han, W., and Cao, Z. (2021). Enhancing the Cycling Stability of Transition-Metal-Oxide-Based Electrochemical Electrode via Pourbaix Diagram Engineering. *Energ. Storage Mater.* 42, 252–258. doi:10.1016/j.ensm.2021.07.037

Javed, M. S., Lei, H., Wang, Z., Liu, B.-t., Cai, X., and Mai, W. (2020). 2D V_2O_5 Nanosheets as a Binder-free High-Energy Cathode for Ultrafast Aqueous and Flexible Zn-Ion Batteries. *Nano Energy* 70, 104573. doi:10.1016/j.nanoen.2020.104573

Javed, M. S., Shah, S. S. A., Najam, T., Siyal, S. H., Hussain, S., Saleem, M., et al. (2020). Achieving High-Energy Density and superior Cyclic Stability in Flexible and Lightweight Pseudocapacitor through Synergic Effects of Binder-free $CoCa_2O_4$ 2D-Hexagonal Nanoplates. *Nano Energy* 77, 105276. doi:10.1016/j.nanoen.2020.105276

Javed, M. S., Shaheen, N., Hussain, S., Li, J., Shah, S. S. A., Abbas, Y., et al. (2019). An Ultra-high Energy Density Flexible Asymmetric Supercapacitor Based on Hierarchical Fabric Decorated with 2D Bimetallic Oxide Nanosheets and MOF-Derived Porous Carbon Polyhedra. *J. Mater. Chem. A.* 7, 946–957. doi:10.1039/c8ta08816k

Jiang, X., Yang, X., Zhu, Y., Shen, J., Fan, K., and Li, C. (2013). *In Situ* assembly of Graphene Sheets-Supported SnS_2 Nanoplates into 3D Macroporous Aerogels for High-Performance Lithium Ion Batteries. *J. Power Sourc.* 237, 178–186. doi:10.1016/j.jpowsour.2013.03.048

Li, X., Zhao, Y., Yao, Q., and Guan, L. (2018). Encapsulating SnS_2 Nanosheets into Hollow Carbon Sphere: A Yolk-Shell SnS_2@C Composite with Enhanced Sodium Storage Performance. *Electrochimica Acta* 270, 1–8. doi:10.1016/j.electacta.2018.03.080

Li, Z., Guo, D., Wang, D., Sun, M., and Sun, H. (2021). Exploration of Metal/Ti_3C_2 MXene-Derived Composites as Anode for High-Performance Zinc-Ion Supercapacitor. *J. Power Sourc.* 506, 230197. doi:10.1016/j.jpowsour.2021.230197

Liu, J. D., Chang, Y. F., Chen, C., Guo, P. Q., Sun, K., Cao, D. L., et al. (2021). Sandwich-like SnS_2/graphene Multilayers for Efficient Lithium/sodium Storage. *Dalton Trans.* 50, 14884–14890. doi:10.1039/d1dt00781e

Parveen, N., Ansari, S. A., Alamri, H. R., Ansari, M. O., Khan, Z., and Cho, M. H. (2018). Facile Synthesis of SnS_2 Nanostructures with Different Morphologies for High-Performance Supercapacitor Applications. *ACS Omega* 3, 1581–1588. doi:10.1021/acsomega.7b01939

Qu, B., Ma, C., Ji, G., Xu, C., Xu, J., Meng, Y. S., et al. (2014). Layered SnS_2-Reduced Graphene Oxide Composite - A High-Capacity, High-Rate, and Long-Cycle Life Sodium-Ion Battery Anode Material. *Adv. Mater.* 26, 3854–3859. doi:10.1002/adma.201306314

Sun, Y., Li, G., Xu, J., Lei, B., Feng, H., and Sun, Z. (2019). Impacts of Graphene Sheets on Photoelectric and Photocatalytic Activities of SnS_2 Nanoparticles. *Mater. Chem. Phys.* 229, 92–97. doi:10.1016/j.matchemphys.2019.02.070

Wang, C., Qu, H., Peng, T., Mei, K., Qiu, Y., Lu, Y., et al. (2016). Large Scale α-$Co(OH)_2$ Needle Arrays Grown on Carbon Nanotube Foams as Free Standing Electrodes for Supercapacitors. *Electrochimica Acta* 191, 133–141. doi:10.1016/j.electacta.2016.01.057

Xie, W., Xu, Z., Zheng, W., Wang, W., Wang, C., Zhang, C., et al. (2021). Fabrication of Ni_3S_2 Nanoneedle-Sheets Electrode Material with Ultrahigh Areal Capacity of over 15 mAh Cm^{-2}. *Mater. Lett.* 282, 128716. doi:10.1016/j.matlet.2020.128716

Zhang, L., Shi, D., Liu, T., Jaroniec, M., and Yu, J. (2019). Nickel-based Materials for Supercapacitors. *Mater. Today* 25, 35–65. doi:10.1016/j.mattod.2018.11.002

Conflict of Interest: The authors declare that the research was conducted in the absence of any commercial or financial relationships that could be construed as a potential conflict of interest.

Publisher's Note: All claims expressed in this article are solely those of the authors and do not necessarily represent those of their affiliated organizations, or those of the publisher, the editors and the reviewers. Any product that may be evaluated in this article, or claim that may be made by its manufacturer, is not guaranteed or endorsed by the publisher.